ChemComm

Chasing Protons in Lithium-Ion Batteries

Journal:	*ChemComm*
Manuscript ID	CC-FEA-07-2022-003970.R1
Article Type:	Feature Article

ARTICLE

Chasing Protons in Lithium-Ion Batteries

Zonghai Chen[a]

Received 00th January 20xx,
Accepted 00th January 20xx

DOI: 10.1039/x0xx00000x

Parasitic reactions between delithiated cathode materials and non-aqueous electrolytes have been a major barrier that limits the upper cutoff potential of cathode materials. It is of great importance to suppress such parasitic reactions to unleash the high-energy-density potential of high voltage cathode materials. Although major effort has been paid to identify the chemical composition of the cathode electrolyte interface using various cutting edge characterization tools, the chemical nature of parasitic reactions remains a puzzle. This severely hinders the rational development of stable high voltage cathode/electrolyte pairs for high-energy density lithium-ion batteries. This feature article highlights our latest effort in understanding the chemical/electrochemical role of cathode electrolyte interface using protons as a chemical tracer for parasitic reactions.

Introduction

Although lithium-ion batteries have been widely considered as the most promising energy storage technology for automobile applications and stationary energy storage, state-of-the-art lithium-ion chemistry is still short of practical specific and volumetric energy density to power long-range electric vehicles (EVs). In the past two decades, various innovative battery materials and engineering solutions have been successfully developed and deployed to continuously improve the practical energy density of lithium-ion batteries. Since the first commercial introduction of lithium-ion battery by Sony Corporation, the amount of charge that can be stored in 18650 cells, 18 mm in diameter and 65 mm in length, has been tripled with up-to-date lithium-ion technologies. Apparently, the physical boundary of each battery component has been significantly pushed to such an extreme that the synergetic effect between different battery components plays an extremely important role to further stretching the performance of lithium-ion chemistries. Therefore, there is a substantially increasing effort in fundamentally understanding the physical/chemical properties of the solid electrolyte interphase (SEI) [1-3], an interfacial layer between the graphitic anode and the electrolyte, and cathode electrolyte interface (CEI) [4-6], an interfacial layer between the cathode material and the electrolyte, with a hope for rationally designing artificial interface to further unlock the energy density of lithium-ion chemistries. Among these effort, major attention has been given to the development of a robust artificial CEI layer to increase the upper cutoff potential of cathode materials to maximize the utilization of precious lithium reservoir in the cathode material and to further improve the practical energy density of the battery [6-8].

With the continuous emergence of advanced surface-sensitive characterization tools, more and more physical and chemical characteristics/fingerprints are available to the community to reconstruct the image of the SEI/CEI layer [9-13]. There is also increasing effort in mapping these characteristics/fingerprints to the performance of the electrode materials and to provide empirical guidance for interface engineering of a better SEI/CEI. However, very limited success was achieved in this area primarily due to the intrinsic drawbacks of

[a] Chemical Sciences and Engineering Division, Argonne National Laboratory, 9700 South Cass Avenue, Lemont, IL 60439, USA. Email: Zonghai.chen@anl.gov

Zonghai Chen is a Senior Chemist at Argonne National Laboratory with 20+ years' experience in developing technologies for high energy-density and high-power lithium and lithium-ion batteries. His research primarily focuses on the behaviour of battery materials at extreme conditions, as well as mass and charge transfer reactions at electrochemically active surface.

these cutting-edge characterization tools. In principle, the modern electron probes and soft X-ray probes are extremely sensitive for probing the physical/chemical properties of interfacial layers. Their low probing depth generally requires an ultrahigh vacuum environment, which can possibly alternate the composition, structure, and functional interface of metastable live SEI/CEI layer [14-16]. In addition, the low energy probing source like electron beam and soft X-ray can also act as an external energy source to trigger unintentional decomposition of CEI layer before a real chemical environment can be detected by the probe [12, 13, 17]. Alternatively, high energy X-ray probes have an excellent penetration capability and little beam damage to the sample, enabling us to probe the real material under realistic conditions, but losing the surface sensitivity. More importantly, the CEI is a layer of organic/inorganic heterogeneous composite material, 10-20 nm in thickness. The functionality of CEI heavily relies on the 3D distribution of these organic/inorganic materials and their intramolecular interactions. Currently, there is not a single damage-free technique that can provide enough chemical sensitivity and spatial resolution to reconstruct the puzzle of a live CEI layer; and hence, a bottom-up design of a highly functional artificial CEI layer remains a great challenge.

Bearing in mind that the core functionality of a working CEI is to minimize the electron transfer reaction between the electrode material and the electrolyte and to maximize the lithium-ion transport across the interface, Dahn's group at Dalhousie University and our team at Argonne National Laboratory pioneered in measuring the functionality of CEI/SEI by developing high precision electrochemical techniques [18, 19]. High precision columbic efficiency (HPCE) measurement was proposed and implemented by Dahn's group to quantitatively measure the loss of active electrons/lithium-ions during a complete charging/discharging cycle as a quantitative indicator of the quality of CEI and SEI layers [20, 21]. At Argonne National Laboratory, we pay more attention to the potential dependent electron transfer reactions between the active electrode materials and the electrolyte by implementing a high precision leakage current (HpLC) measurement [19]. Our 10-year effort in chasing protons using HpLC technique can be rooted back to our early investigation on the thermal decomposition of delithiated cathode materials [22]. With the help of *in situ* high-energy X-ray diffraction (HEXRD) technique, it was found that the onset temperature for the thermal decomposition of $Li_{1-x}Ni_{1/3}Mn_{1/3}Co_{1/3}O_2$ without the presence of non-aqueous electrolyte was about 280°C. With the presence of non-aqueous electrolyte, the onset temperature was significantly reduced to 196°C. This implies that there should be a chemical messager, hypothetically protons [22], to communicate the change of the chemical environment, electrolyte, to the bulk of the crystallized cathode material and to trigger the corresponding change of bulk properties. This hypothesis serves as the cornerstone for our systematic investigation on CEI layer using proton as a chemical tracer.

As will be detailed below, the steady leakage current measured by HpLC can be used as the quantitative indicator of the rate of parasitic reactions, or the rate of the electron transfer reaction between the active material and the electrolyte. It provides chemical insights of parasitic reactions that are not available through other characterization techniques. The following sessions will capture the principle of HpLC, and application of HpLC to track down the proton generation in lithium-ion batteries. The implication of the findings to the field of battery material R&D will also be discussed.

Methodology

It is common that a lithium-ion cell delivers a slightly less capacity during discharge than the charge passes through the cell during the charge stage as shown in Figure 1. The difference is originated from the continuous parasitic reactions between the electrode materials and the electrolyte, causing a small loss of charge stored in the electrode material. This loss of the charge is believed associated with irreversible loss of electrochemical performance during repeating charge/discharge cycling. As shown in insert of Figure 1, the difference between the discharge capacity and

charge capacity is usually less than 0.1% of its reversible capacity. An accurate measurement of this difference can provide a quantitative insight of the rate of the performance loss. This becomes the base for the implementation of HPCE measurement as proposed by Dahn's group [18]. A good relationship between the stable CE and the capacity retention was successfully demonstrated [20]. Apparently, the irreversible capacity loss during charging/discharging is composed of contribution from both the cathode and the anode. Therefore, HPCE measurement is usually conducted on well balanced full cells to eliminating the unpredictable contribution from the metallic lithium anode. It is also clear that the CE measured is an integration of parasitic reactions over the whole course of charging/discharging process. The working potential dependent properties cannot be easily obtained using HPCE measurements. In addition, HPCE approach also lacks the capability to differentiate multiple parasitic reaction pathways as to be discussed next. Table 1 provides a quick comparison between HPCE and HpLC.

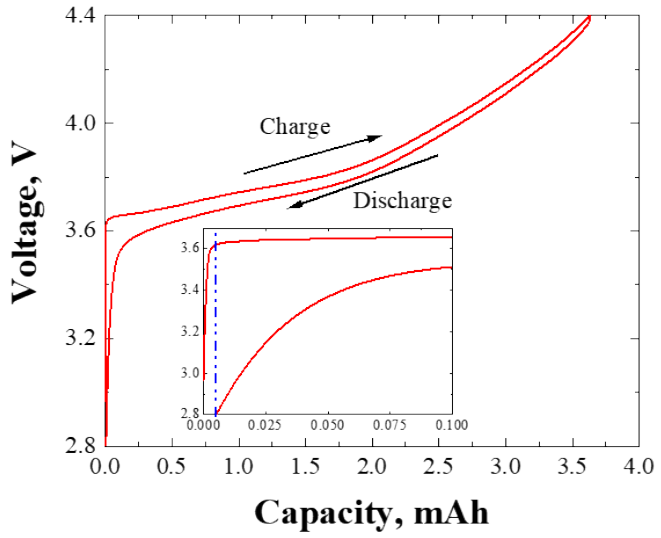

Figure 1 Voltage profile of $Li/LiNi_{0.6}Mn_{0.2}Co_{0.2}O_2$ cell showing a continuous loss of a small fraction of reversible capacity during repeating charge/discharge cycling.

Table 1 A quick comparison between HPCE and HpLC

	HPCE	HpLC
Measuring physics	The amount of charge transfer across the interface.	The rate of charge transfer across the interface.
Testing vehicle	Well balanced full cells	Half cells and full cells
Testing period	Short	Long
Kinetic study	Difficult	Easy
Potential dependent study	Difficult	Easy
Differentiating reaction pathways	No	Yes

Bearing the desire to obtain the potential dependent signal to characterize the chemical nature of the parasitic reactions, our team at Argonne National Laboratory alternatively implemented the HpLC approach to measure the steady leakage current of half cells [19]. As shown in Figure 2a, the core of HpLC measurement is high precision sourcemeters as used for HPCE by Dahn's group. The measuring principle for HpLC is schematically illustrated in Figure 2b; the half-cell is constant voltage held at a specific potential of interest for an extended period, for instance 20 hours, while the current passing through the external circuit is continuous recorded during the constant voltage holding. A typical data collected during this process is shown in Figure 2c. After constant voltage holding for extended period, one can reasonably assume that the concentration gradient of both electrons and lithium ions inside the cell has been eliminated, and the steady leakage current measured is purely contributed from the continuous parasitic reactions that result in continuous electron transfer from the electrolyte to the working electrode.

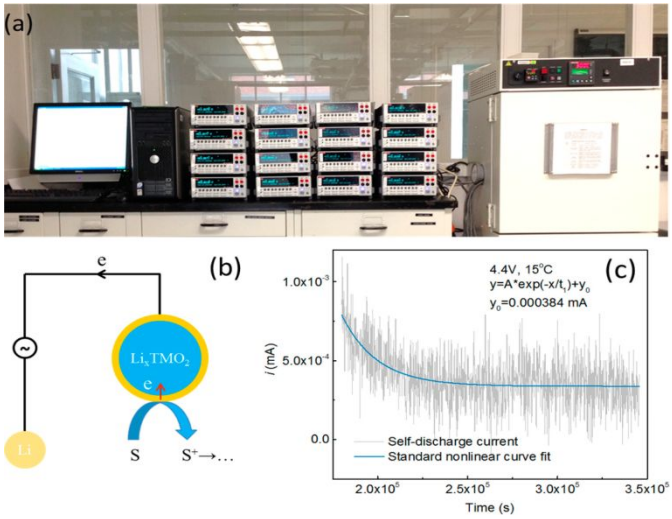

Figure 2 (a) Picture of a 16-channel high precision leakage current measuring system; (b) schematics showing the connection between the leakage current and the rate of parasitic reactions; (c) a typical current relaxation curve collected to extract the static leakage current. [19] Copyright (2016). American Chemical Society.

Clearly, HpLC measurement is only sensitive to any chemical/electrochemical reactions that will change the electrochemical potential of the working electrode; the change of potential is the driving force that the external circuit depends on to quantitative count the amount of charge transfer involved. Consequently, HpLC measurement is intrinsically blind to any chemical/electrochemical reactions with the metallic lithium, which will not alternate the electrochemical potential of the metallic lithium. Therefore, half-cells are ideal for HpLC measurement for an easy control on the potential of the working electrode, and the measured steady leakage current is only contributed from the working electrode. Therefore, the measured steady leakage current can be used as a quantitative indicator of the rate of the parasitic reactions at the given working potential and at the given temperature. This provides us a unique opportunity to investigate the kinetics of parasitic reactions, and to differentiate multiple reaction pathways.

Source of protons

Although commonly accepted by the community that lithium-ion batteries are susceptible to acidic protons, there is an ongoing debate on the source and chemical/electrochemical roles of protons inside a lithium-ion cell. Resolving this argument has been very tricky since the concentration of acidic protons in a nonaqueous environment is usually very low, and their interaction with the battery components is mostly hidden by the dominant intercalation/deintercalation of active electrode materials. Therefore, investigating the charge transfer reaction at a current collector, without the involvement of active electrode material, can provide a clearer picture on the chemical nature of the parasitic reactions [23]. Figure 3a shows a set of steady leakage current measured on a bared aluminium current collector as a function of the working electrode. At the first glance, the steady leakage current increases exponentially with the working potential exponentially (Figure 3a), which is a common behaviour of electrochemical oxidation reaction. Worthy of mentioning is a big gap between 3.8 V and 4.0 V vs. Li^+/Li, the typical raw data at 3.9V are shown as Figure 3b, which clearly shows that the leakage current continuously increase, instead of decrease, with the holding time. This behaviour is against with the traditional electrochemical oxidation reaction, whose current would have decayed exponentially with the experimental time. The only explanation to this unusual behaviour is that the involved electrochemical reaction continuously alternates the surface chemistry of the working electrode, Al foil, resulting in a continuous increase on the exchange current density. As shown in insert of Figure 3a, it is argued that the electrolyte component, mostly ethylene carbonate, is electrochemically oxidized at a relative low potential, resulting in short-life organic radical cations on the surface layer of the Al foil. The newly generated organic radical cations quickly undergo deprotonation reaction to reach its stable state, resulting a locally concentrated proton on the surface layer of the Al foil. The resulted locally concentrated proton can cause the chemical corrosion of the Al_2O_3 layer on the surface of Al foil, causing the improvement on the electron transfer kinetics between the electrolyte and the Al foil between 3.8 V and 4.0V. At the same time, the concentrated proton can also react with $LiPF_6$ to passivate the Al foil

with a layer of AlF_3, driving the interfacial reaction back to normal electrochemical oxidation reaction with a constant exchange current density [23].

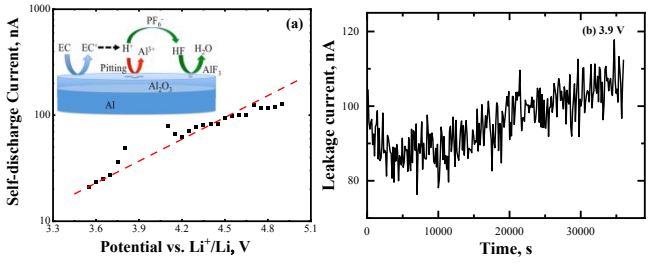

Figure 3 (a) Evolution of the static parasitic current as a function of the holding potential for a dummy Al/Li cell, (b) Evolution of the measured current as a function of the holding time for Al/Li cell at 3.9 V vs. Li^+/Li. [23] The electrolyte used is 1.2 M $LiPF_6$ in EC/EMC (3:7, by mass). Copyright (2017). American Chemical Society.

Above results suggest that the oxidation of carbonate solvents can noticeably occur at a potential as low as 3.8 V vs. Li^+/Li, while experimental measurement using linear scanning voltammetry (LSV) [24] and prediction using density function theory (DFT) calculations [25] also suggest the oxidation potential can be higher than 5.0 V vs. Li^+/Li. DFT calculations predict the standard redox potential of a reversible electrochemical couple, in which case the oxidized specie is kinetically stable and can be reversibly reduced. Nernst Equation (as shown in Equ. 1) describes the relationship between the standard redox potential (ε^0) and the measured redox potential (E).

$$E = \varepsilon^0 + \frac{RT}{nF} ln \frac{[Ox]}{[Red]} \quad (1)$$

In above equation, E is the measured redox potential of the Ox/Red redox couple, ε^0 is the standard redox potential of the redox couple, R is the gas constant, T is the temperature, n is the number of electrons involved in the elemental redox reaction, F is the Faraday constant, [*Ox*] and [*Red*] are the concentrations of oxidized specie and reduced specie, respectively. Clearly, the measured redox potential will be the standard redox potential, as predicted by the DFT calculation, only when [*Ox*]=[*Red*]. In the case of oxidation of carbonate solvents, the oxidized organic radical cation is extremely unstable, and will undergo simultaneous decomposition reaction to release protons. When a steady state, $\frac{\partial[Ox]}{\partial t}$=0, is reached for the electrochemical oxidation of carbonate solvents, the concentration of the oxidized specie can be expressed as Equ. 2.

$$[Ox] = \frac{k_f}{k_b + k_d}[Red] \quad (2)$$

In Equ. 2, k_f is the rate of the forward reaction that oxidizes *Red* into *Ox*; k_b is the rate of the backward reaction that reduces *Ox* back to *Red*; k_d is the rate of the deprotonation reaction that consumes *Ox*. For the case of carbonates, k_f generally equals to k_b while k_d is substantially larger than k_b. By combining Equ. 2 with Equ. 1, one can easily find that the measured redox potential for carbonates will be substantially lower than their thermodynamic standard redox potential as predicted by DFT calculations.

When going back to the HpLC study on Al foil [23], the chemical corrosion of the Al_2O_3 is only observable when the dilution effect of the bulk electrolyte cannot catch up with the rate of the deprotonation reaction, resulting in locally concentrated protons on the surface of Al foil so that a chemical corrosion can occur. This implies that the local concentration of the proton near the electrode surface is more important than the amount of proton in the bulk electrolyte. Therefore, the uniformly generated proton from the moisture impurity in the electrolyte is of less electrochemical importance than those dynamically generated during the operation of batteries.

Role of protons

Given the fact that the dynamically formed protons are electrochemically more important than those uniformly distributed in the electrolyte, it is important to get some insight into the chemical nature of parasitic reactions occurring on the surface of the cathode material. Figure 4a shows a typical dependence of the steady leakage current on the working potential of $LiNi_{0.6}Mn_{0.2}Co_{0.2}O_2$ [19]. Overall, the steady leakage current increase monotonically with the working potential, except for a

quick drop at around 4.5 V vs. Li^+/Li. This behaviour suggests a potential change of the reaction mechanism at about 4.5 V. Therefore, the steady leakage current, equivalent to the rate of parasitic reactions, were measured at different temperatures and different working potential as shown in Figure 4b. Clearly, the kinetic behaviour of the reaction at 4.6 V is different from the one occurs below 4.5 V. Both Arrhenius equation and Tafel equation are independently applied to fit the kinetic data shown in Figure 4b; a constant activation energy was obtained for the parasitic reaction occurs below 4.5 V. This strongly indicates that the parasitic reaction between the delithiated cathode and carbonate molecules below 4.5 V is a chemical reaction [19], unlike the electrochemical oxidation reaction occurs on the surface on Al foil [23]. To gain more chemical insight of the reaction, DFT calculations were also conducted to elucidate the specific interaction between the ethylene carbonate molecule and the interfacial atoms on $LiCoO_2$ cathode [26]. The DFT results indicate that a chemical bonding between the π orbital (C=O) of ethylene carbonates the d orbital of interfacial transition metal (Co) is energetically preferred. Therefore, a layer of carbonate molecules will chemically absorb on the surface of the cathode material using interfacial transition metal atoms as the active absorption sites. The chemical bonding between the carbonate solvent molecules and the cathode material will further facilitate the charge transfer from the carbonate molecules to the cathode material when the cell is charged. Moreover, the chemical bonding at the interface also hinders the diffusion of oxidized specie and/or proton to be diluted by the electrolyte.

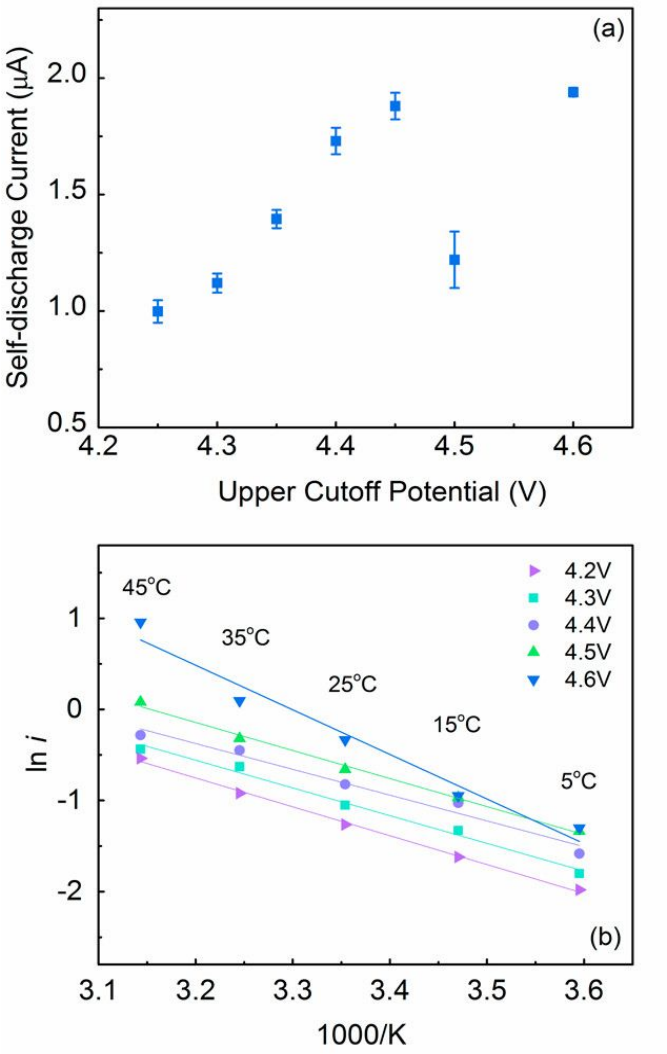

Figure 4 (a) Variation of the static current at 30 °C as a function of the upper cutoff potential, and (b) temperature-dependent static leakage current as a function of the upper cutoff potential [19]. Copyright (2017). American Chemical Society.

The disproportion reaction of Mn(III) into Mn(IV) and Mn(II) was used to explain the dissolution of Mn^{2+} in to the non-aqueous electrolyte. If this is the case, then severe dissolution would occur at a low potential when trivalent transition metal is the major component at the discharged state. Apparently, this hypothesis is against with *in situ* X-ray Absorption Spectroscopy (XAS) reported by Gasteiger's team [27]. Gasteiger et. al. utilized *in situ* XAS to track the concentration of transition metal ions in the electrolyte during the charging process of $LiNi_{0.6}Mn_{0.2}Co_{0.2}O_2$. It was found that the concentration of the transition metal increased with the working

potential of the cathode material, a major increase in concentration of transition metals occurs at around 4.6 V vs. Li^+/Li, which agrees well with the rate of parasitic reactions measured by HpLC [19]. Combing with our previous study on the chemical corrosion of Al foil, it is fair to believe that the dynamically generated locally concentrated proton can also corrode the lithium transition metal oxides, causing the dissolution transition metal ions at a high potential range. Meanwhile, portion of the dynamically generated acidic protons can also diffuse towards electrolyte and eventually reach the negative electrode, causing a slow but continuous decomposition of $LiPF_6$ in the electrolyte [28] and generation of H_2 at the anode side, so called cross talk [29].

Since proton bears the same amount of charge as lithium ion, but with a smaller diameter, it is reasonable to believe that the proton can have a high mobility in layered oxide framework[30, 31], such as delithiated cathode materials [22, 32]. In other word, the insertion of protons into the layered structure is thermodynamically possible. As a matter of fact, the proton is highly mobile in layered β-NiOOH, which is an active cathode material for Nickel hydride batteries [30, 31]. Mimicking the potential acidic environment, Li_2MnO_3 was treated with a weak acidic aqueous solution (pH~4) [32]. After the treatment with an acidic solution, the Li_2MnO_3 powder was recovered and dried for characterization using solid state nuclear magnetic resonance (ss-NMR) and neutron scattering. Clear signal of inserted proton in Li_2MnO_3 was observed by both ss-NMR and neutron scattering. To confirm the electrochemical role of the inserted proton, resonant inelastic X-rat scattering (RIXS) was utilized to probe the chemical environment of oxygen before after charging Li_2MnO_3 to 4.8 V vs. Li^+/Li (see Figure 5). After charging Li_2MnO_3 to 4.8 V, two striking features were observed on O K-edge mapping resonant inelastic X-ray scattering (mRIXS) results. One is the left shoulder at 523.7 eV emission energy, which is well known for the reversible redox of lattice oxygen at a high potential. While the right shoulder at about 527 eV, which is associated with the inserted proton to provide a new charge compensation mechanism for reversible redox of lattice oxygen.

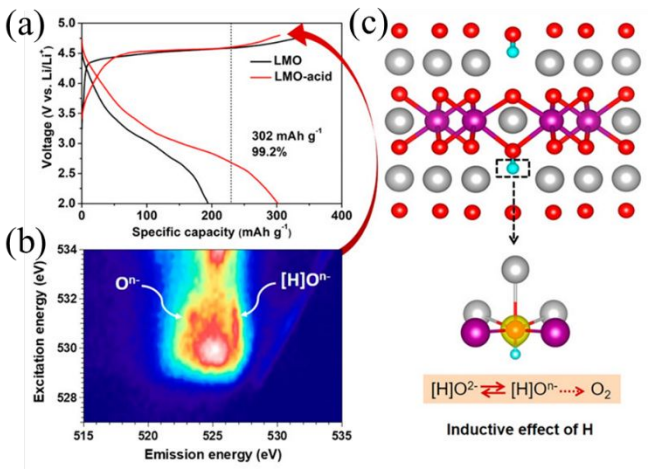

Figure 5 (a) Initial charge/discharge profiles of Li_2MnO_3 with and without acid treatment, (b) O K-edge mapping resonant X-ray scattering (mRIXS) spectra of the acid-treated Li_2MnO_3 after charged to 4.8 V, (c) schematic illustration for the redox reaction with the presence of inserted protons. [32] Copyright (2020). American Chemical Society.

In the open literature, there are plenty of reports on that the chemical modification on the electrolyte or surface coating of cathode material can substantially alternate the bulk properties of the cathode materials. Using *in situ* HEXRD to trace the structural evolution of layered transition metal oxides during charge/discharge cycling, Xu et. al. observed that a spinel-like structure, with a Fd-3m space group, evolved when charging the pristine cathode material to a potential higher than 4.5 V vs. Li^+/Li (see Figure 6a) [33]. This signals an adverse phase transformation during the charging process. By uniformly deposing a thin layer of poly(3,4-ethylenedioxythiophene) (PEDOT) using organic vapor deposition (oCVD), the adverse phase transformation to spinel-like structure was completed eliminated (see Figure 6b), leading to a significant improvement on the capacity retention of the cathode material. Yan et. al. investigated the performance loss mechanism for $LiNi_{0.76}Mn_{0.14}Co_{0.1}O_2$ and found severe intragranular crack after cycling the cathode between 2.7 V and 4.5 V for 200 cycles [34]. To mitigate the cracking issue, a layer

of Li_3PO_4 was coated on the surface of the cathode material via atomic layer deposition (ALD), followed by an annealing at 600°C to allow the infusion of Li_3PO_4 into grain boundaries. With the protection of Li_3PO_4, the intergranular cracking was successfully eliminated, resulting in a major improvement on the capacity retention of the cathode material. Using *in situ* XRD to follow the structural evolution during charging/discharging of $LiCoO_2$, Dahn et. al. confirmed that a H1-3 phase is formed when $LiCoO_2$ is charged to 4.5 V and above [35]. The phase transformation from O3 phase to H1-3 accompanies an intralayer gliding between adjunct CoO_6 layers to form the specific staging of H1-3 phase. This adverse phase transition has been a major barrier for high-voltage cathodes. On the other hand, it was also reported that this adverse phase transition can be mitigated to enable high voltage cycling by either surface coating or simply heat treatment at 550°C [33, 34, 36-38]. Interestingly, Tan et. al. recently reported that a stable cycling of $LiNi_{0.76}Mn_{0.14}Co_{0.1}O_2$ up to 4.8 V can be achieved by adding lithium difluorophosphate as a functional electrolyte additive to passivate the surface of the cathode material [39]. Without any doubt, above examples have made clear statements on the issues associated with the bulk properties of oxide materials, and innovative solutions were also successfully proposed and implemented to address the intended issues. However, the major discrepancy among these examples is the underline mechanism that oxide materials are armed to sense the change of the chemical environment around the oxide particles, either in electrolyte solution or as a surface coating, so that the materials can alternate their bulk behaviour accordingly to reflect the change of the chemical environment. Combining with our study on the parasitic reactions, one can quickly realize that the proton can be the chemical messager to communicate the change of chemical environment to the bulk of oxide materials. Hence, the potential chemical/electrochemical role of protons in layered transition metal oxides deserves more scientific attention to fully elucidate the chemical nature of parasitic reactions between the cathode materials and the electrolyte.

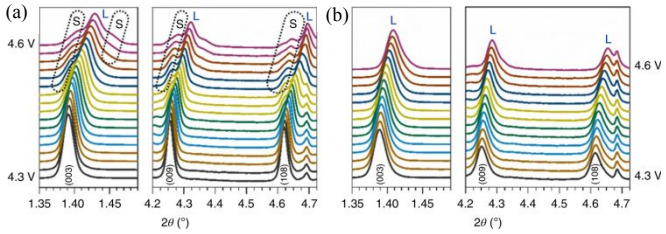

Figure 6 Selected *in situ* high-energy X-ray diffraction patterns of bare NCM111 (a) and 60-PEDOT@NCM111 (b) cathodes in the high-voltage (4.3–4.6 V) region during charge at C/10. L and S in a and b represent layered and spinel-like structures, respectively [33]. Copyright (2019), Springer Nature.

Mitigation strategies

Parasitic reactions at the cathode surface are a series of complicated chemical/electrochemical reactions that are triggered by an electrochemical process, i.e. removal of lithium out of cathode materials that facilitates the electron transfer reactions between the cathode material and an electrolyte component. The oxidized electrolyte component like solvent molecules can then trigger other reactions. Based on our latest work, it is still far away from constructing the full chemical image of parasitic reactions. Figure 7 presents our latest understanding on electrochemically triggered electron transfer reaction [26]. As shown in Figure 7, there are multiple elemental reaction steps involved for the electron transfer from the solvent to the electrode material. Worth of emphasizing is that ethylene carbonate is considered as the point of blame without making a clear differentiation between linear carbonates and cyclic carbonates.

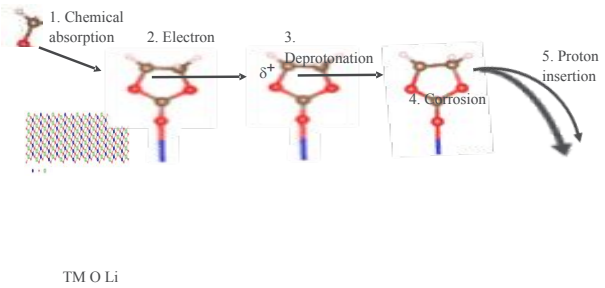

Figure 7 Schematic of elemental reactions for the electron transfer reaction between the carbonate

molecule and the cathode material [26]. Copyright (2019), American Chemical Society.

Chemical absorption of carbonate molecules – When the active cathode material gets into contact with the non-aqueous electrolyte, carbonate solvents will form a chemical bonding between the carbonyl group (C=O π electron pair) with the empty d orbitals of interfacial transition metal ions. Using $LiCoO_2$ as a model system, spin-polarized density functional theory (DFT) calculations clearly shows that ethylene carbonate tends to be chemically absorbed on the surface of $LiCoO_2$ by forming a weak coordination bond between the interfacial Co atoms and the carbonyl group of ethylene carbonate, with a negative change of Gibbs free energy (-0.25 eV). It is also shown that the bonding strength increases with the degree of delithiation of $LiCoO_2$ and that the bond length between the oxygen (in ethylene carbonate) and cobalt (in $LiCoO_2$) monotonically decreases. This clearly suggests that the interfacial transition metal ions are active sites for the chemical absorption of the carbonate solvents [26].

Electron transferring from absorbed solvent to cathode – When the cathode material is charged, lithium and electron are removed from the cathode material, and the Fermi energy level in the cathode material is also reduced accordingly. At a certain stage the difference on the electron energy level between carbonates and the cathode material will be large enough to trigger the migration of electrons from the absorbed molecules to the cathode material through the coordination bond. The rate of the electron transfer reaction depends more on the availability of active sits, oxidized transition metal ions on the surface of the cathode. Therefore, the electron transfer reaction behaves more like a chemical reaction rather than an electrochemical reaction, as reported previously [19].

Deprotonation reaction of oxidized carbonates – When the absorbed carbonate molecule loses an electron to the cathode material, it becomes an extremely unstable organic radical cation, which can be stabilized by undergoing fragmentation reaction and releasing a proton. Making it worse, this deprotonation reaction occurs at a relative high potential when the strong bonding severely hinders the diffusion of the radical cation into the bulk electrolyte. Therefore, the generated protons will be preferentially deposited on the very surface of the cathode material, resulting in a locally concentrated protons for chemical corrosion of oxides, dissolution of transition metal ions [23], and the insertion of protons into the lattice of oxide materials [32].

Accordingly, mitigation solutions to parasitic reactions can be rationally deigned based on above reaction pathways, as summarized in the following paragraphs.

Reducing absorbed carbonate solvents – Since ethylene carbonate is believed to be an important starting reagent for parasitic reactions at the cathode electrolyte interface, the development of low ethylene carbonate or ethylene carbonate free electrolytes has been demonstrated effective to improve the high voltage stability of the cathode electrolyte interface [40-43]. Reducing the number of the active transition metal sites that are exposed to the electrolyte is an alternative approach to slow down the parasitic reactions between the cathode and the electrolyte. For instance, organic cyanides have a terminal -C≡N function group that can form a much stronger coordination bonds with transition metal ions than the carbonyl group in ethylene carbonate. When $LiCoO_2$ was pre-treated with an organic cyanide, the active sites on the cathode surface will be pre-occupied with cyanides, leaving fewer active sites for chemical absorption of ethylene carbonate. Therefore, a substantial reduction in the steady leakage current, or the rate of parasitic reactions, is observed with the poison effect of the organic cyanide [26]. Finally, surface coating of the cathode materials with variety of oxides, fluorides, and phosphates has been the prevailing approach to reduce the exposed transition metal active sites and to improve the electrochemical performance. It has been previously argued that the role of such coating layers is to suppress the parasitic reactions, generating less acidic protons, and requiring less scarifying oxide materials to react with the generated protons [44-47].

Retarding electron transferring – Retarding the electron transfer from the chemically absorbed ethylene carbonate molecules the cathode material is another effective strategy to suppress the parasitic reactions. Partially substituting -H groups with electron withdrawing groups, such as -F groups, has been widely used to improve the high voltage stability of electrolytes [48-51]. Our previous work has shown that a completely replacing ethylene carbonate with difluoroethylene carbonate can significantly reduce the steady leakage current of $LiNi_{0.6}Mn_{0.2}Co_{0.2}O_2$, and leading to great improvement on the long term cycling performance [48]. The same improvement was also observed by replacing both solvents with fluoroethylene carbonate and fluoroethyl methyl carbonate [49].

Hindering interaction between protons and cathode materials – Given that no solution can be perfect, last line of defence will be to slow down the attack of the generated protons and other organic fragments. As argued above, an effective chemical/electrochemical impact of protons can be realized only when a certain level of concentration is reached. Depositing a proton diffusion barrier layer on the intimate surface of the cathode material can be beneficial to slow down the diffusion of protons towards the oxide material, leaving more time for dynamically generated protons to diffuse towards the bulk electrolyte and get diluted. Our previous work has shown that surface coating of Al foil with graphene can substantially suppress the chemical corrosion of Al foil at high potentials [23]. It was also demonstrated that deposition of a poly(3,4-ethylenedioxythiophene) on the cathode surface can also suppress the adverse phase transformation between the layered structure and spinel-like structure. The strategy of polymer coating can also be implemented *in situ* by adding electrochemical active monomers, such as 3-hexylthiophene, as an electrolyte additive to smartly deposit the *in situ* formed polymer on hot spots of the cathode surface [33].

Outlook

In the past decade, we have implemented a high precision leakage current measurement system to quantitatively measure the rate of parasitic reactions between the delithiated cathode and the nonaqueous electrolyte. Particularly, proton is adopted as a chemical tracer to unveil the chemical/electrochemical nature of parasitic reactions. It was identified that the so-called parasitic reactions include at least one chemical oxidation of carbonates, with the help of chemical bonding to facilitate the electron transfer reaction, and at least one direct electrochemical oxidation of carbonates on electronic conducting surface. The construction of reaction pathways for initial charge transfer reactions provides an important guide for rational design of mitigation solutions to suppress parasitic reactions for high voltage cathode materials.

Although some success has been achieved with high precision leakage current measurement, our effort is still far from completing the reconstruction of chemical image of solid electrolyte interface. Given the knowledge on the dynamically generated protons at the high potential region, we still lack knowledge on the residual organic fragments generated after the deprotonation reactions. These organic fragments can either deposit on the hot spots of the cathode materials to prevent further following up undesired parasitic reactions, for example of functional electrolyte additives, or diffuse to the anode side and compromise the electrochemical integrity of the solid electrolyte interphase, generally called crosstalk. Therefore, a fundamental understanding on the nature of these organic fragments and strategically promoting/demoting their electrochemical impact remains a bigger challenge, and opportunity as well, to further unlock the energy density of high voltage cathode materials. Moreover, the mobility and electrochemical roles of protons in lattice of lithium transition metal oxides are still unknown to the community. More research attention is needed to fairly determine the impact of the lattice protons.

Conflicts of interest

There are no conflicts to declare.

Acknowledgements

Research at Argonne National Laboratory was supported by U.S. Department of Energy (DOE), Vehicle Technologies Office and Advanced Manufacturing Office. Argonne National Laboratory is operated for the US Department of Energy by U Chicago Argonne, LLC, under contract DE-AC02-06CH11357.

Notes and references

1. T. Liu, L. Lin, X. Bi, L. Tian, K. Yang, J. Liu, M. Li, Z. Chen, J. Lu, K. Amine, K. Xu and F. Pan, *Nature Nanotechnology*, 2019, **14**, 50-56.
2. J. Tan, J. Matz, P. Dong, J. Shen and M. Ye, *Advanced Energy Materials*, 2021, **11**, 2100046.
3. P. Verma, P. Maire and P. Novák, *Electrochimica Acta*, 2010, **55**, 6332-6341.
4. J. Cabana, B. J. Kwon and L. Hu, *Accounts of Chemical Research*, 2018, **51**, 299-308.
5. D. Chen, M. A. Mahmoud, J.-H. Wang, G. H. Waller, B. Zhao, C. Qu, M. A. El-Sayed and M. Liu, *Nano Letters*, 2019, **19**, 2037-2043.
6. D. Huang, C. Engtrakul, S. Nanayakkara, D. W. Mulder, S.-D. Han, M. Zhou, H. Luo and R. C. Tenent, *ACS Applied Materials & Interfaces*, 2021, **13**, 11930-11939.
7. J. H. Kim, N. P. Pieczonka, P. Lu, Z. Liu, R. Qiao, W. Yang, M. M. Tessema, Y. K. Sun and B. R. Powell, *Advanced Materials Interfaces*, 2015, **2**, 1500109.
8. T. D. Pham and K. K. Lee, *Small*, 2021, **17**, 2100133.
9. Q. Gu, J. A. Kimpton, H. E. Brand, Z. Wang and S. Chou, *Advanced Energy Materials*, 2017, **7**, 1602831.
10. F. Tang, Z. Wu, C. Yang, M. Osenberg, A. Hilger, K. Dong, H. Markötter, I. Manke, F. Sun and L. Chen, *Small Methods*, 2021, **5**, 2100557.
11. D. Atkins, E. Capria, K. Edström, T. Famprikis, A. Grimaud, Q. Jacquet, M. Johnson, A. Matic, P. Norby and H. Reichert, *Advanced Energy Materials*, 2022, **12**, 2102694.
12. Y. Li, Y. Li, A. Pei, K. Yan, Y. Sun, C.-L. Wu, L.-M. Joubert, R. Chin, A. L. Koh and Y. Yu, *Science*, 2017, **358**, 506-510.
13. X. Wang, Y. Li and Y. S. Meng, *Joule*, 2018, **2**, 2225-2234.
14. C. Wang, A. J. Appleby and F. E. Little, *Journal of Electroanalytical Chemistry*, 2001, **497**, 33-46.
15. Z. Chen, Y. Qin, J. Liu and K. Amine, *Electrochemical and Solid-State Letters*, 2009, **12**, A69.
16. Z. Chen, Y. Qin, Y. Ren, W. Lu, C. Orendorff, E. P. Roth and K. Amine, *Energy & Environmental Science*, 2011, **4**, 4023-4030.
17. H. G. Steinrück, C. Cao, M. R. Lukatskaya, C. J. Takacs, G. Wan, D. G. Mackanic, Y. Tsao, J. Zhao, B. A. Helms, K. Xu, O. Borodin, J. F. Wishart and M. F. Toney, *Angew Chem Int Ed Engl*, 2020, **59**, 23180-23187.
18. T. Bond, J. Burns, D. Stevens, H. Dahn and J. Dahn, *Journal of the Electrochemical Society*, 2013, **160**, A521-A527.
19. X. Zeng, G.-L. Xu, Y. Li, X. Luo, F. Maglia, C. Bauer, S. F. Lux, O. Paschos, S.-J. Kim, P. Lamp, J. Lu, K. Amine and Z. Chen, *ACS Applied Materials & Interfaces*, 2016, **8**, 3446-3451.
20. F. Yang, Y. Zhao, K.-L. Tsui and S. j. Bae, *Energy*, 2018, **145**.
21. A. Smith, J. Burns, D. Xiong and J. Dahn, *Journal of The Electrochemical Society*, 2011, **158**, A1136-A1142.
22. Z. Chen, Y. Ren, E. Lee, C. Johnson, Y. Qin and K. Amine, *Advanced Energy Materials*, 2013, **3**, 729-736.
23. T. Ma, G. L. Xu, Y. Li, L. Wang, X. He, J. Zheng, J. Liu, M. H. Engelhard, P. Zapol, L. A. Curtiss, J. Jorne, K. Amine and Z. Chen, *J Phys Chem Lett*, 2017, **8**, 1072-1077.
24. Z. Wang, S. Zhuang, M. Lu and Z. Gong, *Journal of Solid State Electrochemistry*, 2021, **25**, 1353-1360.
25. L. Xing and O. Borodin, *Physical Chemistry Chemical Physics*, 2012, **14**, 12838-12843.
26. Y. Xie, H. Gao, J. Gim, A. T. Ngo, Z.-F. Ma and Z. Chen, *The Journal of Physical Chemistry Letters*, 2019, **10**, 589-594.
27. R. Jung, F. Linsenmann, R. Thomas, J. Wandt, S. Solchenbach, F. Maglia, C. Stinner, M. Tromp and H. A. Gasteiger, *Journal of The Electrochemical Society*, 2019, **166**, A378-A389.
28. D. Strmcnik, I. E. Castelli, J. G. Connell, D. Haering, M. Zorko, P. Martins, P. P. Lopes, B. Genorio, T. Østergaard, H. A. Gasteiger, F. Maglia, B. K. Antonopoulos, V. R. Stamenkovic, J. Rossmeisl and N. M. Markovic, *Nature Catalysis*, 2018, **1**, 255-262.
29. M. Metzger, B. Strehle, S. Solchenbach and H. A. Gasteiger, *Journal of The Electrochemical Society*, 2016, **163**, A798.
30. M. Casas-Cabanas, M. D. Radin, J. Kim, C. P. Grey, A. Van der Ven and M. R. Palacín, *Journal of Materials Chemistry A*, 2018, **6**, 19256-19265.
31. W. Chen, Y. Jin, J. Zhao, N. Liu and Y. Cui, *Proceedings of the National Academy of Sciences*, 2018, **115**, 11694-11699.
32. J. Wu, X. Zhang, S. Zheng, H. Liu, J. Wu, R. Fu, Y. Li, Y. Xiang, R. Liu, W. Zuo, Z. Cui, Q. Wu, S. Wu, Z. Chen, P. Liu, W. Yang and Y. Yang, *ACS Appl Mater Interfaces*, 2020, **12**, 7277-7284.
33. G.-L. Xu, Q. Liu, K. K. S. Lau, Y. Liu, X. Liu, H. Gao, X. Zhou, M. Zhuang, Y. Ren, J. Li, M. Shao, M. Ouyang, F. Pan, Z. Chen, K. Amine and G. Chen, *Nature Energy*, 2019, **4**, 484-494.
34. P. Yan, J. Zheng, J. Liu, B. Wang, X. Cheng, Y. Zhang, X. Sun, C. Wang and J.-G. Zhang, *Nature Energy*, 2018, **3**, 600-605.
35. Z. Chen, Z. Lu and J. R. Dahn, *Journal of The Electrochemical Society*, 2002, **149**, A1604.
36. Z. Chen and J. R. Dahn, *Electrochemical and Solid-State Letters*, 2004, **7**, A11.
37. X. Yang, M. Lin, G. Zheng, J. Wu, X. Wang, F. Ren, W. Zhang, Y. Liao, W. Zhao, Z. Zhang, N. Xu, W. Yang and Y. Yang, *Advanced Functional Materials*, 2020, **30**, 2004664.
38. Z. Chen and J. R. Dahn, *Electrochimica Acta*, 2004, **49**, 1079-1090.
39. S. Tan, Z. Shadike, J. Li, X. Wang, Y. Yang, R. Lin, A. Cresce, J. Hu, A. Hunt, I. Waluyo, L. Ma, F. Monaco, P. Cloetens, J. Xiao, Y. Liu, X.-Q. Yang, K. Xu and E. Hu, *Nature Energy*, 2022, **7**, 484-494.
40. W. Li, A. Dolocan, J. Li, Q. Xie and A. Manthiram, *ECS Meeting Abstracts*, 2019, **MA2019-01**, 263-263.
41. J. R. Dahn, J. Xia, R. Petibon, S. Glazier, K. Nelson, D. Abarbanel, D. Xiong, L. Ellis and A. Louli, *ECS Meeting Abstracts*, 2016, **MA2016-03**, 26-26.
42. L. Ma, S. L. Glazier, R. Petibon, J. Xia, J. M. Peters, Q. Liu, J. Allen, R. N. C. Doig and J. R. Dahn, *Journal of The Electrochemical Society*, 2016, **164**, A5008-A5018.
43. J. Xia, R. Petibon, D. Xiong, L. Ma and J. R. Dahn, *Journal of Power Sources*, 2016, **328**, 124-135.

44. H. Gao, X. Zeng, Y. Hu, V. Tileli, L. Li, Y. Ren, X. Meng, F. Maglia, P. Lamp, S.-J. Kim, K. Amine and Z. Chen, *ACS Applied Energy Materials*, 2018, **1**, 2254-2260.
45. H. Gao, T. Ma, T. Duong, L. Wang, X. He, I. Lyubinetsky, Z. Feng, F. Maglia, P. Lamp, K. Amine and Z. Chen, *Materials Today Energy*, 2018, **7**, 18-26.
46. H. Gao, J. Cai, G.-L. Xu, L. Li, Y. Ren, X. Meng, K. Amine and Z. Chen, *Chemistry of materials*, 2019, **31**, 2723-2730.
47. Z. Chen, D.-J. Lee, Y.-K. Sun and K. Amine, *Mrs Bulletin*, 2011, **36**, 498-505.
48. C.-C. Su, M. He, R. Amine, Z. Chen, R. Sahore, N. D. Rago and K. Amine, *Energy Storage Materials*, 2019, **17**, 284-292.
49. C.-C. Su, M. He, R. Amine, Z. Chen, Z. Yu, T. Rojas, L. Cheng, A. T. Ngo and K. Amine, *Nano Energy*, 2021, **83**, 105843.
50. J. Xia, R. Petibon, A. Xiao, W. M. Lamanna and J. R. Dahn, *Journal of The Electrochemical Society*, 2016, **163**, A1637-A1645.
51. Z. Zhang, L. Hu, H. Wu, W. Weng, M. Koh, P. C. Redfern, L. A. Curtiss and K. Amine, *Energy & Environmental Science*, 2013, **6**, 1806-1810.